

Amide A band is a fingerprint for water dynamics in reverse osmosis polyamide membranes

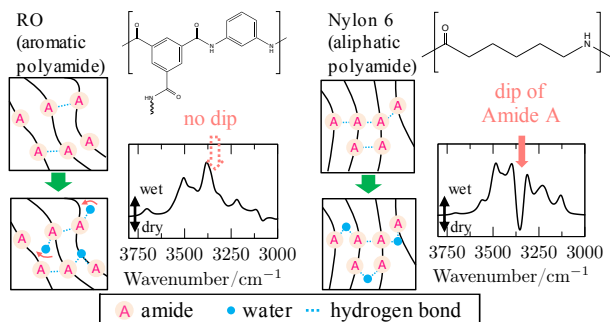
著者	Donatas Surblys, Taro Yamada, Bo Thomsen, Tomonori Kawakami, Isamu Shigemoto, Jun Okabe, Takafumi Ogawa, Masahiro Kimura, Yuji Sugita, Kiyoshi Yagi
journal or publication title	Journal of Membrane Science
volume	596
page range	117705
year	2020-02-15
URL	http://hdl.handle.net/10097/00134305

doi: 10.1016/j.memsci.2019.117705

Graphical Abstract

Amide A Band is a Fingerprint for Water Dynamics in Reverse Osmosis Polyamide Membranes

Donatas Surblys, Taro Yamada, Bo Thomsen, Tomonori Kawakami, Isamu Shigemoto, Jun Okabe, Takafumi Ogawa, Masahiro Kimura, Yuji Sugita, Kiyoshi Yagi



Highlights

Amide A Band is a Fingerprint for Water Dynamics in Reverse Osmosis Polyamide Membranes

Donatas Surblys, Taro Yamada, Bo Thomsen, Tomonori Kawakami, Isamu Shigemoto, Jun Okabe, Takafumi Ogawa, Masahiro Kimura, Yuji Sugita, Kiyoshi Yagi

- A dip of amide A, present in nylon 6, disappears in RO (aromatic polyamides).
- The absence indicates that amide-amide hydrogen bonds (HBs) are kept upon hydration.
- The HB structure facilitates growth of water clusters and rapid water diffusion.
- The amide A band is a fingerprint to probe the water permeability.

Amide A Band is a Fingerprint for Water Dynamics in Reverse Osmosis Polyamide Membranes

Donatas Surblys^a, Taro Yamada^b, Bo Thomsen^a, Tomonori Kawakami^e, Isamu Shigemoto^e, Jun Okabe^f, Takafumi Ogawa^f, Masahiro Kimura^f, Yuji Sugita^{a,c,d} and Kiyoshi Yagi^{a,*}

^aTheoretical Molecular Science Laboratory, RIKEN Cluster for Pioneering Research, 2-1 Hirosawa, Wako, Saitama 351-0198, Japan

^bSurface and Interface Science Laboratory, RIKEN Cluster for Pioneering Research, 2-1 Hirosawa, Wako, Saitama 351-0198, Japan

^cComputational Biophysics Research Team, RIKEN Center for Computational Science, 7-1-26 Minatojima-Minamimachi, Chuo-ku, Kobe, Hyogo 650-0047, Japan

^dLaboratory for Biomolecular Function Simulation, RIKEN Center for Biosystems Dynamics Research, 6-7-1 Minatojima-Minamimachi, Chuo-ku, Kobe, Hyogo 650-0047, Japan

^eAdvanced Materials Research Laboratories, Toray Industries, Inc., 2-1 Sonoyama 3-chome, Otsu, Shiga 520-0842, Japan

^fGlobal Environment Research Laboratories, Toray Industries, Inc., 2-1 Sonoyama 3-chome, Otsu, Shiga, 520-0842, Japan

ARTICLE INFO

Keywords:

IR difference spectrum
Molecular dynamics simulations
Vibrational quasi-degenerate perturbation theory
Amide bands
Water diffusion

ABSTRACT


Reverse osmosis membranes based on aromatic polyamide (ar-PA) are widely used in desalination of seawater, yet the microscopic mechanism of water diffusion through a polyamide layer remains elusive. Here, we study the structure and dynamics of polymer chains and water molecules in ar-PA in comparison to nylon 6 (one of aliphatic polyamides) under various water contents (0.0–15.9 wt%). The infrared (IR) difference spectrum between dry and moist ar-PA shows little change in amide A bands, in contrast to that of nylon 6 which yields a prominent dip. Theoretical analyses using molecular dynamics simulations and quantum electronic and vibrational calculations reveal that the dip in nylon 6 is caused by breaking of hydrogen bonds (HBs) among amide groups. The incoming water molecules that break amide-amide HBs are bound to polyamide chains nearby and diffuse slowly. On the other hand, the amide-amide HBs of ar-PA are kept upon hydration. Such polymer structure facilitates growth of large water clusters with more than 100 water molecules and rapid diffusion of water molecules. The amide A band serves as a fingerprint to characterize the water permeability of polyamide materials.

1. Introduction

Supply of clean water for all is an urgent subject for sustainable development of the global society. Reverse osmosis (RO) desalination is one of the major technologies to produce fresh water from sea and brackish water [1–4]. The process utilizes a RO membrane, which permeates water molecules but rejects other solutes and ions. The feed water is filtered through the membrane with an external pressure applied from the higher salt concentration to the lower against the osmotic pressure. There are various types of RO membranes proposed and developed to date, e.g., cellulose acetate, inorganic/ceramic, and thin film composite (TFC) membranes based on aromatic polyamides (ar-PA) (Fig. 1 (a)).

The TFC membrane consists of three layers: a functionally active ar-PA layer (~ 100 nm thickness), a porous polysulfone support (~ 50 μ m thickness), and a polyester support backing. The ar-PA layer is prepared on the support via interfacial polymerization (IP) reactions of aromatic amines and acyl halides in aqueous and organic solvents, respectively. Cadotte [5, 6] first utilized IP reactions to fabricate the TFC membrane and discovered the effectiveness of ar-PA synthesized from *m*-phenylenediamine (MPD) and trimesoyl chloride (TMC). It was a breakthrough invention that achieved high salt rejection rate of over 99 % while keeping high operational pressure of several MPa. Further improvements have been made by fine tuning the condition of IP reactions [7–10]. Recently, Chowdhury et al. [11] have proposed a novel synthesis method in place of IP, which employs an electrospray to deposit nano-droplets of monomers onto a support, thereby enabling precise control of the thickness and the surface roughness of ar-PA layers.

The microscopic structure of ar-PA has been investigated with great interest, because the filtration involves atomic and molecular processes that require a delicate balance between permeability and selectivity [12]. The observation using atomic force microscopy (AFM) has revealed that the surface of ar-PA has a ridge-and-valley structure with a

 kiyoshi.yagi@riken.jp (K. Yagi)
ORCID(s):

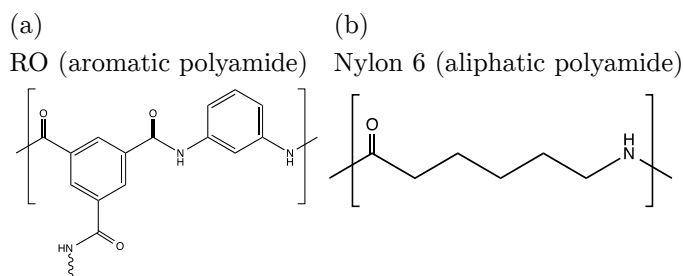


Figure 1: The chemical structure of (a) RO aromatic polyamide and (b) aliphatic polyamide or nylon 6.

roughness of ~ 50 nm [13]. The pore size has been measured to be in a range of 2 – 3 Å by positron annihilation lifetime spectroscopy (PALS) [14–17]. Lee et al. [18] characterized the water vapor sorption of ar-PA and measured the variation of pore size with respect to the water content using PALS. The chemical composition and the degree of cross-linking have been obtained by X-ray photoelectron spectroscopy (XPS) and Rutherford backscattering spectrometry (RBS) [19]. Jin et al. [20] measured infrared (IR) spectra during the water absorption process suggesting that the hydration of ar-PA takes place in two steps. Theoretical calculations using all-atom molecular dynamics (MD) simulations have been performed for a hydrated ar-PA system. The pioneering work by Kotelyanskii et al. [21, 22] has revealed that water molecules diffuse in “jump-like” movements inside ar-PA. A number of works have followed with improved structural modeling of ar-PA and advanced simulation techniques [23–31]. The interaction between a polymer and water molecules has been investigated by analyzing the radial distribution functions (RDF), the number of hydrogen bonds (HBs) in a polymer, and so on [32–34]. Recently, non-equilibrium molecular dynamics (NEMD) simulations have been carried out to calculate transport properties through an ar-PA membrane in the presence of water flow [35–39].

In the present study, we focus on the diffusion of water molecules in ar-PA in comparison to nylon 6, which is one of aliphatic polyamides (Fig. 1 (b)). Because the diffusion coefficient is related to the water permeability of a polymer [40], it is one of the critical parameters to judge the applicability of a material to RO filtration. Interestingly, the diffusion coefficient of water molecules is orders of magnitude different between ar-PA and nylon 6. Such a difference may be surprising, given that they are both polyamides with a similar number of carbon atoms (*i.e.*, 5 or 6) between amide groups. Although the low water diffusion of nylon 6 has been suggested to be due to its partial crystallization [41], we have recently found in MD simulations that the diffusion of water molecules in nylon 6 is already slow in amorphous, non-crystallized systems [42]. Therefore, nylon 6 serves as a good counterpart of ar-PA to understand the molecular mechanism for water diffusion in polyamide materials.

To elucidate the dynamics of water molecules in ar-PA, we have carried out IR spectroscopic measurements and theoretical calculations. IR spectroscopy is a powerful method for this purpose due to its high sensitivity to hydrogen bonds (HBs). The amide groups give rise to strong bands in IR spectra originating from C=O stretching, C–N–H bending, C–N stretching, and N–H stretching vibrational modes, which are commonly referred to as amide I, II, III, and A bands, respectively. Upon the formation of HBs, the amide bands show characteristic change in position and intensity, thereby serving as a reporter of HB networks. It has been extensively used to probe the secondary structure of protein [43, 44], amyloid fibril formation [45], and so on. The calculations have been performed to assign the observed vibrational bands. We have recently developed a weight average method, which combines structural samplings using all-atom MD simulations and anharmonic vibrational theory based on quantum chemical calculations [46, 47]. In the previous work [42], we applied the method to nylon 6 to show that the incorporation of various HB structures and anharmonic vibrational motion yields reliable computational IR spectra of hydrated polymer materials.

In the following, we first show the result of MD simulations of ar-PA and the IR difference spectra between dry and moist ar-PA. The IR spectra obtained by experiment and theory are compared to assess the accuracy of the calculation and to assign the nature of vibrational bands. Then, we discuss the hydration structure and the mechanism of water diffusion by highlighting the differences in the interaction between polymer chains and water molecules in ar-PA and nylon 6. We show that HB networks of amide groups play key role to promote the growth of large water molecules in ar-PA, which facilitates rapid diffusion of water molecules in ar-PA. Amide A bands in IR difference spectra characterize the HB networks, and help the design of novel polyamide materials with high the water permeability.

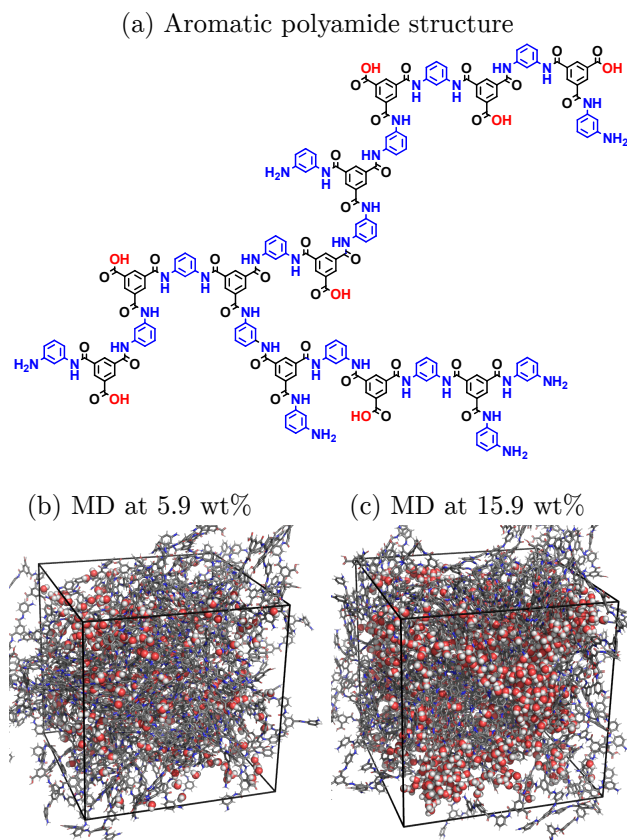


Figure 2: (a) A chain of ar-PA used in MD simulations taken from Ref. 34. The chemical composition is $C_{195}H_{142}N_{32}O_{40}$. (b) and (c) Snapshot structures of a system with the water content of 5.9 and 15.9 wt%. Each system contains 32 chains of ar-PA.

2. Methods

Computational and experimental methods are briefly described below. Further details are found in the supporting information (SI).

2.1. Molecular dynamics

The atomistic structure of hydrated ar-PA was created based on a model of the RO membrane developed by Kawakami et al. [34]. The chemical structure of a single polymer chain is shown in Fig. 2 (a). A dry system was first prepared using 32 polymer chains. Then, water molecules were inserted in the system using PACKMOL [48], so as to set the water content to target values, 3.1, 5.9, 8.6, and 15.9 wt%.

The LAMMPS [49] simulation package was used to perform all-atom MD simulations. We used the force field parameters of ar-PA developed in the previous work [34], and TIP3P [50] for water molecules. The MD simulation was carried out for 40 ns with timesteps of 1 fs in the constant temperature and pressure ensemble at 300 K and 1 atm with Nosé-Hoover thermostats and barostats each with three chains [51]. For computing the self-diffusion coefficients of water molecules, another MD simulation was performed for 60 ns in the constant volume and temperature ensemble at 300 K using the Bussi thermostat [52]. The short-range interaction was cut off at 10 Å, and the long-range Coulomb interaction was treated with PPPM [53] at the precision of 10^{-5} in LAMMPS. The RATTLE [54] algorithm was used to constrain bonds containing hydrogen atoms and H–O–H angles of water molecules. The snapshot structures of the system thus obtained are shown in Fig. 2 (b,c).

2.2. Weight averaged anharmonic vibrational calculations

The method is explained in Ref. 47. The distinguishing feature of the method is that it combines quantum electronic and vibrational calculations with classical MD simulations, which makes it feasible to compute accurate anharmonic vibrational spectrum with an account of structural samplings. In brief, MD simulations are first carried out to sample the structure, and the resulting structures are classified into molecular clusters that contribute to the vibrational spectrum. Then, the cluster is modeled in the gas phase, and the vibrational spectrum is calculated for each cluster by anharmonic vibrational methods combined with the electronic structure theory. Finally, the total spectrum is obtained by a weight average over the spectra of clusters. The method has been applied to a lipid bilayer [46], a phosphate ion in solution [55], and nylon 6 [42].

In this study, the clustering was performed in terms of HB patterns. HB patterns of fragments of ar-PA (benzanilide, aniline, and benzoic acid) and water molecules [see Fig. S1 (a) in SI] were investigated through MD trajectories to obtain HB clusters and their statistical weights. The HB bond length was derived for all pairs of elements from number density distribution functions (see Section S1.2 of SI). Then, density functional theory (DFT) calculations were carried out for the clusters at the level of B3LYP [56, 57] functional and 6-31++G(d,p) basis sets using Gaussian09 [58]. Following the geometry optimization and harmonic vibrational analysis, the potential energy surface (PES) and the dipole moment surface (DMS) were computed by a grid method using 11 grid points along each coordinate up to two-mode coupling levels [59]. The vibrational Schrödinger equation was solved by the second-order vibrational quasi-degenerate perturbation theory (VQDPT2) [60, 61] to obtain the vibrational energy levels and the IR intensities. Anharmonic vibrational program, SINDO developed by us [62], was used to generate the PES and DMS, and to perform VQDPT2 calculations. Finally, the total IR spectrum was obtained by a weight average of VQDPT2 spectra over all the clusters.

2.3. Trajectory analysis

The volume of pores and the space of water molecules needed to obtain the porosity was computed using the GROMACS free volume analysis program [63]. The probe radius and the number of probe insertions were set to 0.0 Å and 10 Å⁻³, respectively, for each trajectory snapshot. The distribution of pore size was computed using the PSDSolv program [64]. The program was slightly modified to incorporate the periodic boundary condition and to set the probe insertion number in the input. The number of probe insertions and the minimal probe radius were set to 1 Å⁻³ and 0.0 Å, respectively. 80 samples were used to estimate the standard deviation for each water content value. D^{wat} was obtained from the Einstein relation. The mean square displacement (MSD) was calculated up to 60 ns, and the slope was obtained by a linear fitting in a region of 18 – 60 ns. Further details as well as plots of MSD are given in SI.

2.4. Fourier transform (FT) IR measurement

The RO membrane samples for ambience-controlled FTIR measurement were formed on infrared-transparent Si wafer pieces. The RO membrane samples (thickness 1 – 5 μm) were fabricated over pieces of Si wafers by liquid interfacial polymerization. The spectral recording was performed in a pure N₂-purged compartment of a FTIR spectrometer equipped with a silicon barometer IR detector. Two identical light paths were composed with IR-transparent Si wafer windows for the sample and the background in a gas-tight container. The sample spectrum and the background spectrum were recorded separately, and the background cancellation was conducted by numerical processing.

The gas-tight container was filled with dry N₂ or humidity-controlled H₂O in N₂ during FTIR measurement. For precise humidity control, the cell was charged with H₂O/glycerol mixtures for desired humidity, and allowed for a few hours for equilibration. It is known that H₂O/glycerol system equilibrates the ambient space in the full range of relative humidity at the room temperature and in the vicinity. The humidity and temperature within the container were always monitored with a compact electronic thermo/hygrometer. The humidity was converted to the water content using a relation reported in Ref. 34.

3. Results and discussion

3.1. Properties of ar-PA in different hydration levels

The density of ar-PA, the self-diffusion coefficient of water molecules (D^{wat}), and the porosity obtained from MD simulations are listed in Table 1. The porosity is calculated by

$$\Phi^{\text{type}} = \frac{N^{\text{type}}}{N} \times 100\%, \quad (1)$$

Table 1

The mass density of a polymer (ρ^{poly}), the number density of amide groups (n^{amid}) and water molecules (n^{wat}), the self-diffusion coefficient of water molecules (D^{wat}), and the porosity (Φ^{vac} , $\Phi^{\text{vac+water}}$) obtained from MD simulations with different water contents.

ar-PA					
water content (wt%)	0.0	3.1	5.9	8.6	15.9
ρ^{poly} (g/cm ³)	1.30	1.27	1.24	1.20	1.08
n^{amid} (nm ⁻³)	5.71	5.58	5.43	5.27	4.75
n^{wat} (nm ⁻³)	0.00	1.34	2.61	3.80	6.85
D^{wat} ($\times 10^{-7}$ cm ² /s)	—	0.19	0.46	0.90	4.69
Φ^{vac} (%)	34.39	33.59	33.19	32.86	33.60
$\Phi^{\text{vac+wat}}$ (%)	34.39	35.83	37.56	39.26	45.24
Nylon 6 ^a					
water content (wt%)	0.0	2.3	4.5	8.6	15.9
ρ^{poly} (g/cm ³)	1.09	1.07	1.05	1.01	0.93
n^{amid} (nm ⁻³)	5.67	5.55	5.46	5.27	4.86
n^{wat} (nm ⁻³)	0.00	0.85	1.65	3.19	5.89
D^{wat} ($\times 10^{-7}$ cm ² /s)	—	0.015	0.014	0.057	0.28
Φ^{vac} (%)	33.91	34.01	33.60	33.25	33.47
$\Phi^{\text{vac+wat}}$ (%)	33.91	35.35	36.22	38.36	43.06

^a Ref.42.

where N is the total number of probe insertion attempts, and N^{type} with type = “vac” and “vac+wat” is the number of successful probe insertions into the pores and pores or volume covered by water molecules, which is also proportional to the volume ratio of pores, and that of pores and water molecules, respectively.

As the water content increases from 0.0 to 15.9 wt%, the density of ar-PA (ρ^{poly}) steadily decreases from 1.30 to 1.08 g/cm³. These values agree with experimental ones for FT-30, which were reported to be 1.24 and 1.06 g/cm³ at 11.2 and 23 wt%, respectively [21, 65].

D^{wat} is obtained in a range of 0.19×10^{-7} to 4.69×10^{-7} cm²/s, which is two orders of magnitude smaller than that of bulk water (5.06×10^{-5} cm²/s for the TIP3P water model [66]). Thus, the diffusion of water molecules is significantly slower in the RO membrane than in the bulk. It is notable that the increase in the water content leads to a substantial increase in D^{wat} . To confirm this trend, we further carried out a MD simulation for a system with the water content of 23 wt%, and obtained D^{wat} as 2.29×10^{-6} cm²/s. This result is consistent with the previous reports. D^{wat} was obtained in a range of $2 - 5 \times 10^{-6}$ cm²/s in the previous MD simulations with the same water content (23 wt%) [24–28, 32]. In experiment, it was estimated to be $1 - 8 \times 10^{-6}$ cm²/s [65] based on the solution-diffusion model [40].

As the water content increases, Φ^{vac} remains approximately 34 % with little change, whereas $\Phi^{\text{vac+wat}}$ shows a steady increase up to 45 %. The result suggests that water molecules form clusters in a membrane that grow large along with an increase in water contents, instead of occupying the pores.

3.2. IR difference spectra

Theoretical and experimental IR difference spectra between dry and moist ar-PA are shown in Fig. 3 (see SI for the absolute spectrum). Note that the dry system is taken to be 5.9 wt% and 6.3 wt% in theory and experiment, respectively, because removal of water molecules from the RO membrane down to 0.0 wt% was difficult in experiment. The calculated spectrum agrees well with the experiment reproducing major dips and peaks. As shown in the bottom panel of Fig. 3 (a), the experimental spectrum yields a large, broad band in a high frequency range, which matches well with that of bulk water. Thus, it is plausible to assign the band to O–H stretching vibration of water molecules. The calculated spectrum supports this assignment. The decomposition of the spectrum, shown in the upper panel of Fig. 3 (a), indicates that the O–H stretching modes of water molecules mainly contribute to this band. It is notable that only half of the intensity is ascribed to water molecules surrounded by water, and that the other half originates from water molecules hydrogen bonded to ar-PA. Interestingly, the amide A band is too weak to be visible in the IR difference spectrum.

In a low frequency range, the decomposition of the calculated spectrum identifies amide I, II, and III of ar-PA, which are labeled as I, II, and III, respectively, in the upper panel of Fig. 3 (b). All of them come in pairs of a dip and

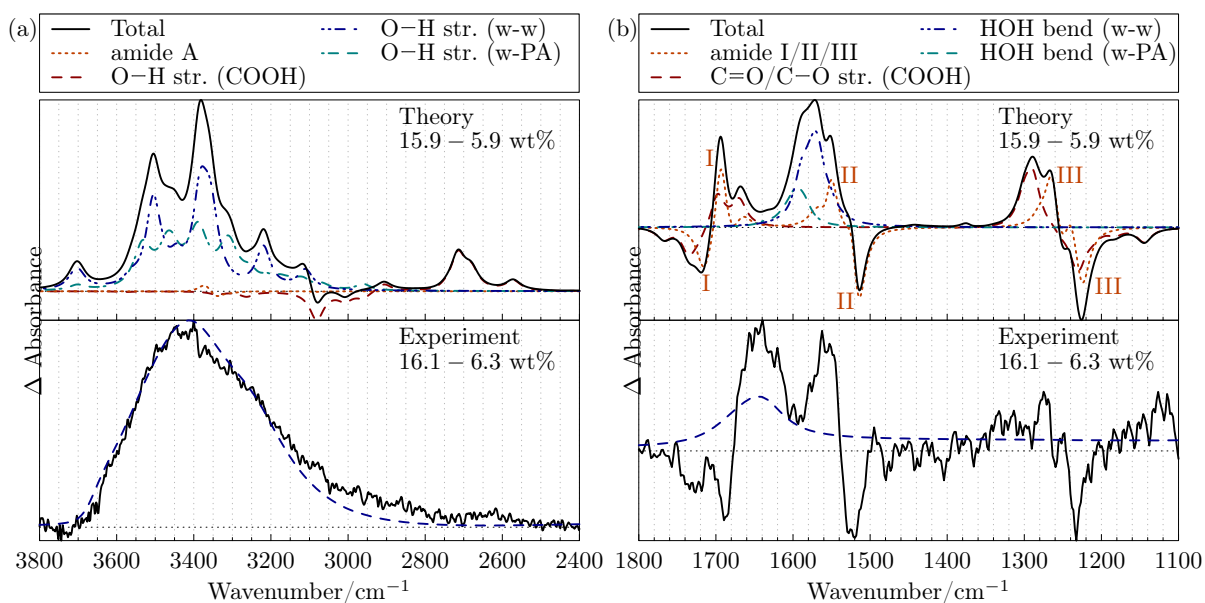


Figure 3: Theoretical and experimental IR difference spectra of ar-PA in (a) high and (b) low frequency ranges. The total spectrum of bulk water [67] is also superimposed with dotted lines in the experimental ones. The calculated spectrum (solid line) is decomposed into the contribution from water molecules interacting with other water molecules (w-w) and ar-PA (w-PA), the amide groups of ar-PA, and the carboxyl groups (COOH). The position of amide I, II, and III are indicated by labels I, II, and III, respectively.

a peak, indicating the loss of amide groups without water and the formation of hydrated amide groups. Note that the peak is lower in frequency than the dip for amide I, whereas the order is reversed for amide II and III. This is because the HB between amide groups and water molecules weakens the C=O bond and leads to a red-shift of amide I. On the other hand, the bending motion of C–N–H is restricted and the C=NH stretching motion is strengthened due to the formation of HBs, thereby leading to a blue-shift of amide II and III.

A discrepancy between theory and experiment is seen for an intensity ratio of two peaks in a range of 1500 – 1700 cm^{-1} . The first peak around 1640 cm^{-1} is more intense than the second one around 1560 cm^{-1} in experiment, whereas the second peak is more intense than the first one in the calculated spectrum. The source is traced to the bending vibration of water molecules. The IR spectrum of bulk water, also shown in the bottom panel of Fig. 3 (b), gives the water bending band around 1640 cm^{-1} , which matches well with the first band in the experiment. On the other hand, the water bending band is calculated to be lower in frequency around 1570 – 1600 cm^{-1} . The underestimate may be due to the limited accuracy of quantum chemistry calculations.

The carboxylic acid group has pKa commonly below 5 in water solution, and thus is believed to exist as a deprotonated carboxylate anion near the interface between water and ar-PA at neutral pH. The carboxylate anion charges the surface of ar-PA negatively, and has substantial effect on ion rejection capabilities [68, 69]. However, the protonation state is less clear in the membrane, in particular, upon water uptake. In Fig. 3 (b), the C=O stretching mode of the carboxylic acid is clearly observed as a dip at 1720 cm^{-1} in both experiment and theory. The C–O stretching band calculated in a range of 1200 – 1300 cm^{-1} is hardly discerned in the total spectrum due to an overlap with amide III. Nevertheless, the shape of the calculated spectrum resembles with the experimental one, exhibiting a sharp dip at 1220 cm^{-1} and a relatively broad peak around 1280 cm^{-1} . The O–H stretching mode gives a dip and a peak around 3100 and 2700 cm^{-1} , respectively, in the calculated spectrum in Fig. 3 (a). The dip is assigned to the loss of HBs between a carboxyl group and an amide group of ar-PA, while the peak arises from a hydrated carboxyl group. The peak is also observed in the experimental spectrum around 2600 cm^{-1} , though it is less prominent compared to the calculated spectrum. On the other hand, the experimental spectrum in Fig. 3 (b) lacks in any distinct bands in the 1400 cm^{-1} region, where the C=O stretching modes of carboxylate anions should give rise to [70]. These results indicate that the carboxyl group remains protonated even in a moist membrane without substantial change in the population of carboxy-

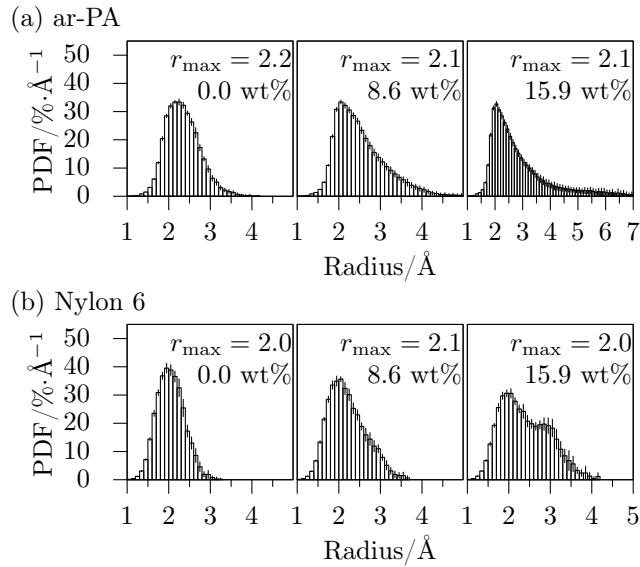


Figure 4: Probability distribution function (PDF) of the size of pores and water molecules in (a) ar-PA and (b) nylon 6. PDFs in each panel are normalized so that the integral matches the porosity of pores and water molecules ($\Phi^{\text{vac}+\text{water}}$) in Table 1. The radius at the maximum is displayed as r_{max} .

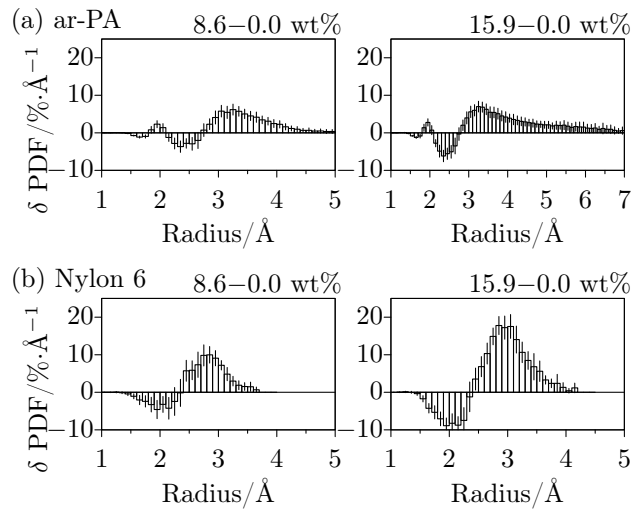


Figure 5: Difference PDF from 0.0 wt% in (a) ar-PA and (b) nylon 6.

late anions. This finding is in accordance with the previous experiment, which demonstrated for a wide variety of RO membranes that the ionization behavior is explained well by two types of carboxyl groups with significantly different pKa values [19, 71–73].

3.3. Comparison of ar-PA and nylon 6

In this section, we discuss on the hydration structure of ar-PA and nylon 6, and its relation to D^{wat} . The properties of nylon 6 calculated in the previous work [42] are listed in Table 1. Although the mass and number densities of nylon 6 are similar to those of ar-PA, D^{wat} is more than ten times different between the two. The difference has also been observed in experiment: D^{wat} of RO and nylon 6 has been reported to be $1 - 8 \times 10^{-6} \text{ cm}^2/\text{s}$ [65] and $0.5 - 3 \times 10^{-8} \text{ cm}^2/\text{s}$ [74, 75], respectively.

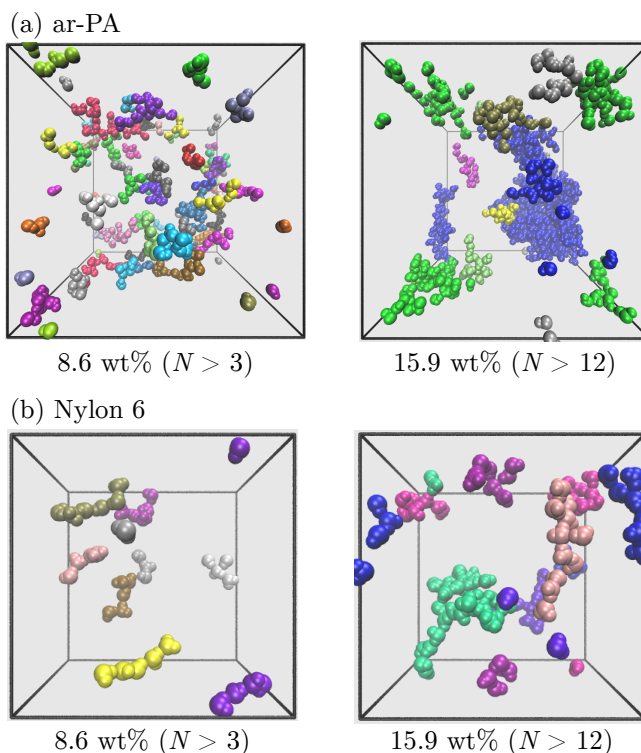


Figure 6: Snapshots of water clusters in (a) ar-PA and (b) nylon 6. Water molecules in the same cluster are represented with the same color. The clusters with the number of water molecules (N) smaller than 3 and 12 are not shown for clarity for 8.6 and 15.9 wt%, respectively. Note that the system volume is roughly 8 times different (twice in dimension) between ar-PA and nylon 6.

Fig. 4 shows the probability distribution functions (PDFs) of the size of pores and water molecules for ar-PA and nylon 6 with water contents of 0.0, 8.6, and 15.9 wt%. In dry systems, the PDFs of ar-PA and nylon 6 both show a single Gaussian peak with the maximum radius of 2.2 and 2.0 Å, respectively. The maximum radius agrees well with the free volume radius measured around ~ 2.5 Å by PALS experiments [18, 76]. It is notable that the main peaks at $r = 2.0 - 2.1$ Å are retained in moist systems as well, suggesting that the majority of pores remains free from water molecules even after the hydration. This is reinforced by observing that PDFs of the size of "pores only" remain unchanged in dry and moist systems (see Section S2.1 and Fig. S5 in SI).

In Fig. 4, the moist systems show a notable increase in PDF in a long range (i.e., $r \geq 3.0$ Å). To clarify the difference, we have subtracted the PDF of dry systems from that of moist systems. The difference PDF (δ PDF) thus obtained is shown in Fig. 5. δ PDF is found to be negative in a short range and positive in a long range, indicating the loss of pores and the growth of water clusters, respectively. In the long range, ar-PA shows a positive peak around ~ 3.2 Å and a tail that decays slowly and continues as long as 7 Å in the case of 15.9 wt%. In contrast, nylon 6 shows a strong positive peak around 2.8 – 3.0 Å, which decays to zero around 4 Å. The result indicates that ar-PA forms large water clusters, whereas nylon 6 has many small clusters. It is also notable that the radius where δ PDF changes its sign from negative to positive occurs around 2.8 and 2.4 Å in ar-PA and nylon 6, respectively. The turnover radius may be interpreted as the minimum size that water molecules can access in a polymer, thereby suggesting that water molecules access to smaller pores in nylon 6 than in ar-PA.

Water clusters in ar-PA and nylon 6 are visualized in Fig. 6. It is clear that water clusters in nylon 6 prefer to have a long, linear shape. In 15.9 wt%, the largest nylon 6 cluster (shown in green, 33 water molecules) is still elongated, even though it is partly becoming three-dimensional. In striking contrast, some of the water clusters in ar-PA already form three-dimensional shapes at 8.6 wt%. These clusters get connected and gather to form extremely large clusters at 15.9 wt%. The largest (in blue) and the second largest (in green) clusters have 589 and 112 water molecules, respectively. The HB network of water molecules leads to an increase in the self-diffusion coefficient of water molecules. These

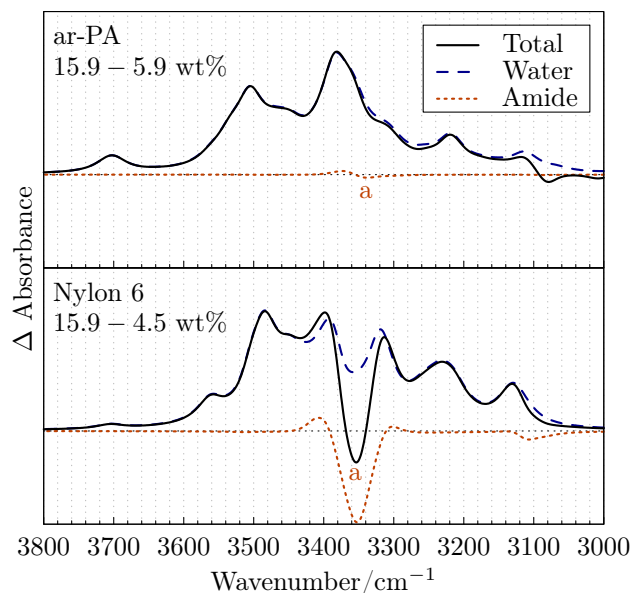


Figure 7: Theoretical IR difference spectrum of ar-PA (this work) and nylon 6 (Ref. 42). The total spectrum (solid black) is decomposed in terms of amide A and O–H stretching modes of water molecules shown in dotted orange and dashed blue lines, respectively.

findings are in line with the previous MD works [31–33], which have reported that large clusters in a polymer with 300 – 600 water molecules facilitate the diffusion of water molecules without the cage effect of polymer environment.

Next, we focus on the IR spectrum to see if the difference in the hydration structure of ar-PA and nylon 6 gives rise to any characteristic signal. A striking difference is observed in a high frequency range of the IR difference spectrum shown in Fig. 7. A strong dip is observed around 3350 cm^{-1} for nylon 6, whereas no such dip is observed for ar-PA. The sharp dip was also observed in the IR measurement of nylon 6 by Iwamoto and Murase [77]. The decomposed spectrum, also shown in Fig. 7, indicates that the dip originates from amide A, *i.e.* the N–H stretching mode of amide groups. Interestingly, ar-PA shows very little changes in amide A. The IR intensities of amide A of nylon 6 and ar-PA are on an equal order. For example, trimers of *N*-methylacetamide and benzanilide, which are one of the major clusters in nylon 6 and ar-PA, yield the IR intensity of amide A as 663 and 238 km/mol , respectively. Therefore, the absence of the dip in ar-PA is not due the IR intensity of amide A, but indicates a difference in the hydration structure of amide groups.

Amide groups and water molecules classified in terms of their HB types are displayed in Fig. 8. In the right panel of Fig. 8 (a), the number of amide groups in nylon 6 that have no HBs with a polymer (red area), is only 0.72 nm^{-3} at 0.0 wt %, but dramatically increases to 2.59 nm^{-3} at 15.9 wt%. The change is mainly caused by a decrease of amide groups that form HBs with a polymer both as an acceptor and a donor (blue area), where the number varies from 2.55 nm^{-3} to 0.42 nm^{-3} . The result indicates that dry nylon 6 has well developed networks of amide-amide HBs, yet the HBs are broken by water molecules upon hydration. This is mirrored in HB types of water molecules in nylon 6. In the right panel of Fig. 8 (b), more than 80 % of water molecules in nylon 6 interact with a polymer (yellow, blue, and white area) in all water contents. Also, the water molecules forming HBs with a polymer both as an acceptor and a donor (blue area) are dominant in low water contents. The result implies a replacement of amide-amide HBs with amide-water HBs. The loss of the amide-amide HBs gives rise to the dip of amide A in the IR difference spectrum.

In contrast, dry ar-PA has less number of HBs among amide groups. The left panel of Fig. 8 (a) shows that the amide groups at 0.0 wt% that form HBs with a polymer as an acceptor and a donor (blue area) are only 1.03 nm^{-3} , whereas those that remain free from HBs (red area) are as much as 1.90 nm^{-3} . The breaking of HBs is observed as the water content increases, but to a much lesser extent than in nylon 6. The extension of red area is 0.67 nm^{-3} and the decrease of blue area is 0.70 nm^{-3} between 0.0 and 15.9 wt%. Note also that 45.0 % of the amide groups are out of contact from water molecules (non-hatched area) even at 15.9 wt%. In ar-PA, the HB networks of amide groups are

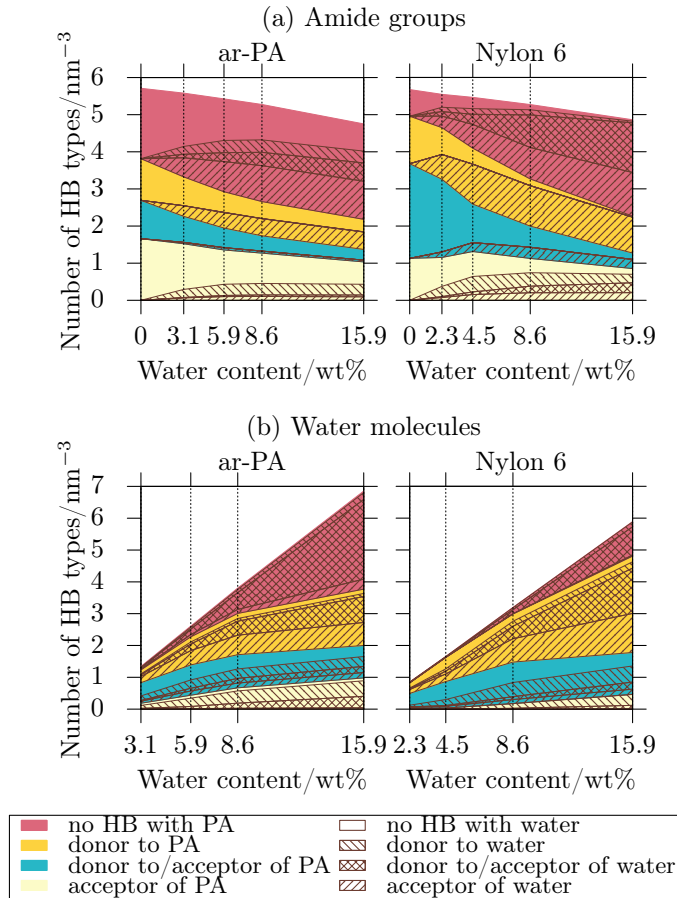


Figure 8: Hydrogen bond analysis of (a) amide groups and (b) water molecules. The results of ar-PA and nylon 6 are displayed in the left and right panels, respectively. The color and the hatched pattern represent HB types formed with a polyamide (*i.e.* amide, carboxyl, and amine groups) and water molecules, respectively.

kept after hydration, thereby suppressing a dip of amide A in the IR difference spectrum.

It is notable in the left panel of Fig. 8 (b) that water molecules in ar-PA that have no HBs with a polymer (red area) steadily grow in number to reach 3.08 nm^{-3} at 15.9 wt %, and that such water molecules form HBs with each other. The result reinforces the growth of water clusters and the development of water-water HB networks in a polymer seen in Fig. 6 (a).

From these results, we propose a mechanism for water diffusion in a polyamide material mediated by HB networks of amide groups, which is schematically illustrated in Fig. 9. In dry ar-PA, the number of HBs among amide groups is relatively few (Fig. 9 (a), left panel). Thus, in the early stage of hydration, water molecules interact with amide groups while retaining certain mobility (Fig. 9 (a), middle panel). As the water content increases, the mobile water molecules facilitate the formation of water clusters and water-water HB networks, which makes rapid diffusion of water molecules feasible through a polymer (Fig. 9 (a) right panel). On the other hand, the HB networks of amide groups are well developed in nylon 6 (Fig. 9 (b), left panel). Water molecules that enter into this network break the HBs between amide groups (Fig. 9 (b), middle panel); the loss of amide-amide HBs signals the dip of amide A. However, such water molecules form multiple HBs with amide groups and have little mobility. Consequently, the growth of water clusters is suppressed (Fig. 9 (b), right panel), leading to an order of magnitude smaller D^{wat} than that of ar-PA. We emphasize that such interaction between water molecules and polyamides can be experimentally characterized by measuring the amide A region in IR spectra.

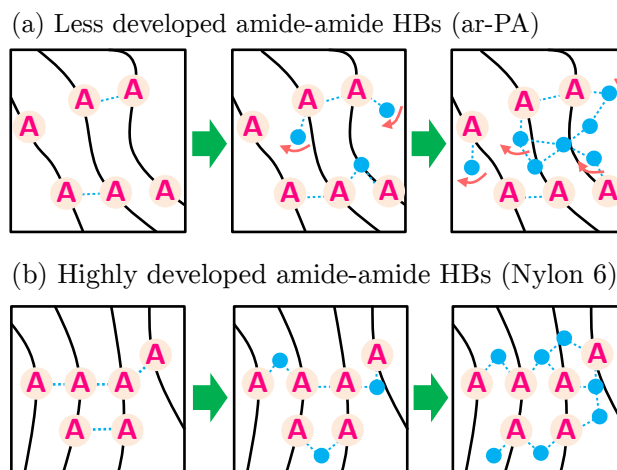


Figure 9: Schematic drawing of water diffusion through HB networks of amide groups. 'A' and blue circles represent amide groups and water molecules, respectively. Black solid and blue dotted lines are polymer chains and hydrogen bonds, respectively. Arrows indicate mobile water molecules that facilitate fast water diffusion in a polymer.

4. Conclusions

The dynamics of water molecules and the interaction with ar-PA are investigated by IR difference spectroscopy, MD simulations, and anharmonic vibrational calculations. The modeling and calculation methods are first validated by comparing the results of MD with available experimental data, and by comparing the computational and experimental IR spectroscopy. Then, the mechanism for water diffusion in ar-PA is discussed in comparison to nylon 6. The analysis of MD trajectories has revealed that ar-PA has fewer number of HBs between amide groups than nylon 6. Such amide-amide HB network enables to recruit mobile water molecules in polyamide and promote the growth of large water clusters, through which water molecules diffuse efficiently. The extent of HB networks among amide groups is characterized by the presence or absence of a dip of amide A bands upon hydration. The present result suggests that the amide A band serves as a marker to indicate the water permeation performance of polyamide materials.

Further study on other polyamide materials is necessary to establish the relation of the amide A band and the water diffusion. For example, ar-PAs with different branching ratio, those before and after degradation, etc. are among the most important ones. The filtration performance is determined not only by the water permeation but also the selectivity. A similar approach combining MD simulations and vibrational spectroscopy is applicable to surface/interface systems, which will reveal the mechanism for ion rejection and fouling. These subjects will be the scope of future works.

Acknowledgements

This research is supported by Japan Science and Technology Agency, COI Grant Number JPMJCE1316. This research is partially supported by the "Integrated Lipidology" and "Dynamic Structural Biology" projects (to Y. Sugita), and the incentive research grant (to K. Yagi) in RIKEN, and JSPS KAKENHI Grant JP26220807 and JP26119006 (to Y. Sugita). B.T. was supported by the Special Postdoctoral Researchers Program at RIKEN. Computational resources were provided by HOKUSAI GreatWave at RIKEN.

A. Supplementary material

Supplementary data associated with this article can be found online at xxx.

References

- [1] D. Li, H. Wang, Recent developments in reverse osmosis desalination membranes, *J. Mater. Chem.* 20 (2010) 4551–4566.
- [2] K. P. Lee, T. C. Arnot, D. Mattia, A review of reverse osmosis membrane materials for desalination - Development to date and future potential, *J. Membr. Sci.* 370 (2011) 1 – 22.

- [3] W. Lau, A. Ismail, N. Misdan, M. Kassim, A recent progress in thin film composite membrane: A review, *Desalination* 287 (2012) 190 – 199.
- [4] S. S. Shenvi, A. M. Isloor, A. Ismail, A review on RO membrane technology: Developments and challenges, *Desalination* 368 (2015) 10 – 26.
- [5] J. E. Cadotte, Reverse osmosis membrane, 1977. US Patent 4039440.
- [6] J. E. Cadotte, Interfacially synthesized reverse osmosis membrane, 1981. US Patent 4277344.
- [7] A. K. Ghosh, B.-H. Jeong, X. Huang, E. M. Hoek, Impacts of reaction and curing conditions on polyamide composite reverse osmosis membrane properties, *J. Membr. Sci.* 311 (2008) 34 – 45.
- [8] B. Khorshidi, T. Thundat, B. A. Fleck, M. Sadrzadeh, Thin film composite polyamide membranes: parametric study on the influence of synthesis conditions, *RSC Adv.* 5 (2015) 54985–54997.
- [9] B. Khorshidi, T. Thundat, B. A. Fleck, M. Sadrzadeh, A novel approach toward fabrication of high performance thin film composite polyamide membranes, *Sci. Rep.* 6 (2016) 22069.
- [10] Z. Tan, S. Chen, X. Peng, L. Zhang, C. Gao, Polyamide membranes with nanoscale Turing structures for water purification, *Science* 360 (2018) 518–521.
- [11] M. R. Chowdhury, J. Steffes, B. D. Huey, J. R. McCutcheon, 3D printed polyamide membranes for desalination, *Science* 361 (2018) 682–686.
- [12] H. B. Park, J. Kameev, L. M. Robeson, M. Elimelech, B. D. Freeman, Maximizing the right stuff: The trade-off between membrane permeability and selectivity, *Science* 356 (2017) 1138–1148.
- [13] S.-Y. Kwak, S. G. Jung, Y. S. Yoon, D. W. Ihm, Details of surface features in aromatic polyamide reverse osmosis membranes characterized by scanning electron and atomic force microscopy, *J. Polym. Sci. B: Polym. Phys.* 37 (1999) 1429–1440.
- [14] A. Shimazu, K. Ikeda, T. Miyazaki, Y. Ito, Application of positron annihilation technique to reverse osmosis membrane materials, *Radiat. Phys. Chem.* 58 (2000) 555 – 561.
- [15] S. H. Kim, S.-Y. Kwak, T. Suzuki, Positron annihilation spectroscopic evidence to demonstrate the flux-enhancement mechanism in morphology-controlled thin-film-composite (TFC) membrane, *Environ. Sci. Technol.* 39 (2005) 1764–1770.
- [16] Z. Chen, K. Ito, H. Yanagishita, N. Oshima, R. Suzuki, Y. Kobayashi, Correlation study between free-volume holes and molecular separations of composite membranes for reverse osmosis processes by means of variable-energy positron annihilation techniques, *J. Phys. Chem. C* 115 (2011) 18055–18060.
- [17] T. Fujioka, N. Oshima, R. Suzuki, W. E. Price, L. D. Nghiem, Probing the internal structure of reverse osmosis membranes by positron annihilation spectroscopy: Gaining more insight into the transport of water and small solutes, *J. Membr. Sci.* 486 (2015) 106–118.
- [18] J. Lee, C. M. Doherty, A. J. Hill, S. E. Kentish, Water vapor sorption and free volume in the aromatic polyamide layer of reverse osmosis membranes, *J. Membr. Sci.* 425–426 (2013) 217 – 226.
- [19] O. Coronell, B. J. Mariñas, D. G. Cahill, Depth heterogeneity of fully aromatic polyamide active layers in reverse osmosis and nanofiltration membranes, *Environ. Sci. Technol.* 45 (2011) 4513–4520.
- [20] Y. Jin, W. Wang, Z. Su, Spectroscopic study on water diffusion in aromatic polyamide thin film, *J. Membr. Sci.* 379 (2011) 121–130.
- [21] M. Kotelyanskii, N. Wagner, M. Paulaitis, Atomistic simulation of water and salt transport in the reverse osmosis membrane FT-30, *J. Membr. Sci.* 139 (1998) 1 – 16.
- [22] M. Kotelyanskii, N. Wagner, M. Paulaitis, Molecular dynamics simulation study of the mechanisms of water diffusion in a hydrated, amorphous polyamide, *Comp. Theor. Polym. Sci.* 9 (1999) 301 – 306.
- [23] E. Harder, D. E. Walters, Y. D. Bodnar, R. S. Faibish, B. Roux, Molecular dynamics study of a polymeric reverse osmosis membrane, *J. Phys. Chem. B* 113 (2009) 10177–10182.
- [24] Y. Luo, E. Harder, R. S. Faibish, B. Roux, Computer simulations of water flux and salt permeability of the reverse osmosis FT-30 aromatic polyamide membrane, *J. Membr. Sci.* 384 (2011) 1 – 9.
- [25] Z. E. Hughes, J. D. Gale, A computational investigation of the properties of a reverse osmosis membrane, *J. Mater. Chem.* 20 (2010) 7788–7799.
- [26] Z. E. Hughes, J. D. Gale, Molecular dynamics simulations of the interactions of potential foulant molecules and a reverse osmosis membrane, *J. Mater. Chem.* 22 (2012) 175–184.
- [27] M. Ding, A. Ghoufi, A. Szymczyk, Molecular simulations of polyamide reverse osmosis membranes, *Desalination* 343 (2014) 48 – 53.
- [28] V. Kolev, V. Freger, Hydration, porosity and water dynamics in the polyamide layer of reverse osmosis membranes: A molecular dynamics study, *Polymer* 55 (2014) 1420 – 1426.
- [29] V. Kolev, V. Freger, Molecular dynamics investigation of ion sorption and permeation in desalination membranes, *J. Phys. Chem. B* 119 (2015) 14168–14179.
- [30] T. Araki, R. Cruz-Silva, S. Tejima, K. Takeuchi, T. Hayashi, S. Inukai, T. Noguchi, A. Tanioka, T. Kawaguchi, M. Terrones, M. Endo, Molecular dynamics study of carbon nanotubes/polyamide reverse osmosis membranes: Polymerization, structure, and hydration, *ACS Appl. Mater. Interfaces* 7 (2015) 24566–24575.
- [31] T. Wei, L. Zhang, H. Zhao, H. Ma, M. S. J. Sajib, H. Jiang, S. Murad, Aromatic Polyamide Reverse-Osmosis Membrane: An Atomistic Molecular Dynamics Simulation, *J. Phys. Chem. B* 120 (2016) 10311–10318.
- [32] M. Ding, A. Szymczyk, F. Goujon, A. Soldera, A. Ghoufi, Structure and dynamics of water confined in a polyamide reverse-osmosis membrane: A molecular-simulation study, *J. Membr. Sci.* 458 (2014) 236 – 244.
- [33] N. Zhang, S. Chen, B. Yang, J. Huo, X. Zhang, J. Bao, X. Ruan, G. He, Effect of hydrogen-bonding interaction on the arrangement and dynamics of water confined in a polyamide membrane: A molecular dynamics simulation, *J. Phys. Chem. B* 122 (2018) 4719–4728.
- [34] T. Kawakami, M. Nakada, H. Shimura, K. Okada, M. Kimura, Hydration structure of reverse osmosis membranes studied via neutron scattering and atomistic molecular simulation, *Polym. J.* 50 (2018) 327 – 336.
- [35] M. Ding, A. Szymczyk, A. Ghoufi, On the structure and rejection of ions by a polyamide membrane in pressure-driven molecular dynamics simulations, *Desalination* 368 (2015) 76–80.
- [36] W. Gao, F. She, J. Zhang, L. F. Dumée, L. He, P. D. Hodgson, L. Kong, Understanding water and ion transport behaviour and permeability

- through poly(amide) thin film composite membrane, *J. Membr. Sci.* 487 (2015) 32 – 39.
- [37] M. Shen, S. Keten, R. M. Lueptow, Dynamics of water and solute transport in polymeric reverse osmosis membranes via molecular dynamics simulations, *J. Membr. Sci.* 506 (2016) 95 – 108.
- [38] Y. Song, F. Xu, M. Wei, Y. Wang, Water flow inside polyamide reverse osmosis membranes: A non-equilibrium molecular dynamics study, *J. Phys. Chem. B* 121 (2017) 1715–1722.
- [39] K. Li, L. Liu, H. Wu, S. Li, C. Yu, Y. Zhou, W. Huang, D. Yan, Understanding the temperature effect on transport dynamics and structures in polyamide reverse osmosis system: Via molecular dynamics simulations, *Phys. Chem. Chem. Phys.* 20 (2018) 29996–30005.
- [40] J. Wijmans, R. Baker, The solution-diffusion model: a review, *J. Membr. Sci.* 107 (1995) 1 – 21.
- [41] N. S. Murthy, Hydrogen bonding, mobility, and structural transitions in aliphatic polyamides, *J. Polym. Sci. B: Polym. Phys.* 44 (2006) 1763–1782.
- [42] B. Thomsen, T. Kawakami, I. Shigemoto, Y. Sugita, K. Yagi, Weight-averaged anharmonic vibrational analysis of hydration structures of polyamide 6, *J. Phys. Chem. B* 121 (2017) 6050–6063.
- [43] A. Barth, Infrared spectroscopy of proteins, *Biochim. Biophys. Acta* 1767 (2007) 1073–1101.
- [44] Z. Ganim, H. S. Chung, A. W. Smith, L. P. Deflores, K. C. Jones, A. Tokmakoff, Amide I two-dimensional infrared spectroscopy of proteins, *Acc. Chem. Res.* 41 (2008) 432–441.
- [45] C. T. Middleton, P. Marek, P. Cao, C. Chiu, S. Singh, A. M. Woys, J. J. de Pablo, D. P. Raleigh, M. T. Zanni, Two-dimensional infrared spectroscopy reveals the complex behaviour of an amyloid fibril inhibitor, *Nat. Chem.* 4 (2012) 355–360.
- [46] K. Yagi, P.-C. Li, K. Shirota, T. Kobayashi, Y. Sugita, A weight averaged approach for predicting amide vibrational bands of a sphingomyelin bilayer, *Phys. Chem. Chem. Phys.* 17 (2015) 29113–29123.
- [47] K. Yagi, H. Otaki, P.-C. Li, B. Thomsen, Y. Sugita, Weight averaged anharmonic vibrational calculations: Applications to polypeptide, lipid bilayers, and polymer materials, in: Y. Ozaki, J. M. Wojcik, J. Popp (Eds.), *Molecular Spectroscopy: A Quantum Chemistry Approach*, volume 1, Wiley-VCH Verlag GmbH & Co. KGaA, 2019, pp. 147–170.
- [48] L. Martínez, R. Andrade, E. G. Birgin, J. M. Martínez, Packmol: A package for building initial configurations for molecular dynamics simulations, *J. Comput. Chem.* 30 (2009) 2157–2164.
- [49] S. Plimpton, Fast parallel algorithms for short-range molecular dynamics, *J. Comput. Phys.* 117 (1995) 1 – 19.
- [50] W. L. Jorgensen, J. Chandrasekhar, J. D. Madura, R. W. Impey, M. L. Klein, Comparison of simple potential functions for simulating liquid water, *J. Chem. Phys.* 79 (1983) 926–935.
- [51] W. Shinoda, M. Shiga, M. Mikami, Rapid estimation of elastic constants by molecular dynamics simulation under constant stress, *Phys. Rev. B* 69 (2004) 134103.
- [52] G. Bussi, D. Donadio, M. Parrinello, Canonical sampling through velocity rescaling, *J. Chem. Phys.* 126 (2007) 014101.
- [53] R. W. Hockney, J. W. Eastwood, *Computer Simulation Using Particles*, Taylor & Francis, Inc., Bristol, PA, USA, 1988.
- [54] H. C. Andersen, Rattle: A “velocity” version of the shake algorithm for molecular dynamics calculations, *J. Comput. Phys.* 52 (1983) 24 – 34.
- [55] K. Yagi, K. Yamada, C. Kobayashi, Y. Sugita, Anharmonic vibrational analysis of biomolecules and solvated molecules using hybrid QM/MM computations, *J. Chem. Theory Comput.* 15 (2019) 1924–1938.
- [56] C. Lee, W. Yang, R. G. Parr, Development of the Colle-Salvetti correlation-energy formula into a functional of the electron density, *Phys. Rev. B* 37 (1988) 785–789.
- [57] A. D. Becke, Density-functional thermochemistry. III. The role of exact exchange, *J. Chem. Phys.* 98 (1993) 5648–5652.
- [58] M. J. Frisch, G. W. Trucks, H. B. Schlegel, G. E. Scuseria, M. A. Robb, J. R. Cheeseman, G. Scalmani, V. Barone, B. Mennucci, G. A. Petersson, H. Nakatsuji, M. Caricato, X. Li, H. P. Hratchian, A. F. Izmaylov, J. Bloino, G. Zheng, J. L. Sonnenberg, M. Hada, M. Ehara, K. Toyota, R. Fukuda, J. Hasegawa, M. Ishida, T. Nakajima, Y. Honda, O. Kitao, H. Nakai, T. Vreven, J. A. Montgomery, Jr., J. E. Peralta, F. Ogliaro, M. Bearpark, J. J. Heyd, E. Brothers, K. N. Kudin, V. N. Staroverov, R. Kobayashi, J. Normand, K. Raghavachari, A. Rendell, J. C. Burant, S. S. Iyengar, J. Tomasi, M. Cossi, N. Rega, J. M. Millam, M. Klene, J. E. Knox, J. B. Cross, V. Bakken, C. Adamo, J. Jaramillo, R. Gomperts, R. E. Stratmann, O. Yazyev, A. J. Austin, R. Cammi, C. Pomelli, J. W. Ochterski, R. L. Martin, K. Morokuma, V. G. Zakrzewski, G. A. Voth, P. Salvador, J. J. Dannenberg, S. Dapprich, A. D. Daniels, Ö. Farkas, J. B. Foresman, J. V. Ortiz, J. Cioslowski, D. J. Fox, *Gaussian 09 Revision E.01*, 2009. Gaussian Inc. Wallingford CT.
- [59] K. Yagi, S. Hirata, K. Hirao, Multiresolution potential energy surfaces for vibrational state calculations, *Theor. Chem. Acc.* 118 (2007) 681–691.
- [60] K. Yagi, S. Hirata, K. Hirao, Vibrational quasi-degenerate perturbation theory: Applications to fermi resonance in CO₂, H₂CO, and C₆H₆, *Phys. Chem. Chem. Phys.* 10 (2008) 1781–1788.
- [61] K. Yagi, H. Otaki, Vibrational quasi-degenerate perturbation theory with optimized coordinates: Applications to ethylene and trans-1,3-butadiene, *J. Chem. Phys.* 140 (2014) 84113.
- [62] K. Yagi, SINDO 4.0, 2019. <https://tms.riken.jp/en/research/software/sindo/>.
- [63] M. J. Abraham, T. Murtola, R. Schulz, S. Páll, J. C. Smith, B. Hess, E. Lindahl, Gromacs: High performance molecular simulations through multi-level parallelism from laptops to supercomputers, *SoftwareX* 1-2 (2015) 19 – 25.
- [64] S. Bhattacharya, K. E. Gubbins, Fast method for computing pore size distributions of model materials, *Langmuir* 22 (2006) 7726–7731.
- [65] X. Zhang, D. G. Cahill, O. Coronell, B. J. Mariñas, Absorption of water in the active layer of reverse osmosis membranes, *J. Membr. Sci.* 331 (2009) 143 – 151.
- [66] M. W. Mahoney, W. L. Jorgensen, Diffusion constant of the TIP5P model of liquid water, *J. Chem. Phys.* 114 (2001) 363–366.
- [67] J. E. Bertie, Z. Lan, Infrared intensities of liquids XX: The intensity of the OH stretching band of liquid water revisited, and the best current values of the optical constants of H₂O(l) at 25°C between 15,000 and 1 cm⁻¹, *Appl. Spectrosc.* 50 (1996) 1047–1057.
- [68] A. E. Childress, M. Elimelech, Effect of solution chemistry on the surface charge of polymeric reverse osmosis and nanofiltration membranes, *J. Membr. Sci.* 119 (1996) 253 – 268.

- [69] J. Wang, D. S. Dlamini, A. K. Mishra, M. T. M. Pendergast, M. C. Wong, B. B. Mamba, V. Freger, A. R. Verliefe, E. M. Hoek, A critical review of transport through osmotic membranes, *J. Membr. Sci.* 454 (2014) 516–537.
- [70] K. Nakanishi, P. Solomon, *Infrared Absorption Spectroscopy*, Holden-Day, 1977.
- [71] O. Coronell, B. J. Mariñas, X. Zhang, D. G. Cahill, Quantification of functional groups and modeling of their ionization behavior in the active layer of FT30 reverse osmosis membrane, *Environ. Sci. Technol.* 42 (2008) 5260–5266.
- [72] O. Coronell, B. J. M. , D. G. Cahill, Accessibility and ion exchange stoichiometry of ionized carboxylic groups in the active layer of FT30 reverse osmosis membrane, *Environ. Sci. Technol.* 43 (2009) 5042–5048.
- [73] O. Coronell, M. I. González, B. J. Mariñas, D. G. Cahill, Ionization behavior, stoichiometry of association, and accessibility of functional groups in the active layers of reverse osmosis and nanofiltration membranes, *Environ. Sci. Technol.* 44 (2010) 6808–6814.
- [74] L. Monson, M. Braunwarth, C. W. Extrand, Moisture absorption by various polyamides and their associated dimensional changes, *J. Appl. Polym. Sci.* 107 (2008) 355–363.
- [75] N. J. W. Reuvers, H. P. Huinink, H. R. Fischer, O. C. G. Adan, Quantitative water uptake study in thin Nylon-6 films with NMR imaging, *Macromolecules* 45 (2012) 1937–1945.
- [76] J. J. Singh, T. L. Clair, W. H. Holt, W. Mock, Moisture dependence of positron annihilation spectra in nylon-6, *Nucl. Instr. Meth. Phys. Res.* 221 (1984) 427 – 432.
- [77] R. Iwamoto, H. Murase, Infrared spectroscopic study of the interactions of Nylon-6 with water, *J. Polym. Sci. B Polym. Phys.* 41 (2003) 1722–1729.